Three-Dimensional Reconstruction of the 70S *Escherichia coli* Ribosome in Ice: The Distribution of Ribosomal RNA

Joachim Frank,*‡, Pawel Penczek,*§ Robert Grassucci,* and Suman Srivastava*

*Wadsworth Center for Laboratories and Research, Empire State Plaza, Albany, New York 12201-0509; ‡Department of Biomedical Sciences, State University of New York at Albany, Albany, New York 12201; §Institute of Experimental Physics, Warsaw University, Warsaw, Poland

Abstract. A reconstruction, at 40 Å, of the *Escherichia coli* ribosome imaged by cryo-electron microscopy, obtained from 303 projections by a single-particle method of reconstruction, shows the two subunits with unprecedented clarity. In the interior of the subunits, a complex distribution of higher mass density is recognized, which is attributed to ribosomal RNA. The masses corresponding to the 16S and 23S components are linked in the region of the platform of the small subunit. Thus the topography of the rRNA regions responsible for protein synthesis can be described.

THE ribosome is a highly complex organelle, formed by assembly of proteins and nucleic acids, and responsible for protein synthesis in all organisms. Knowledge of its structure, even at moderate resolution, will help to unravel the numerous steps in the translation of the genetic message into a polypeptide chain. Models of the ribosome that were derived by visual interpretation of electron micrographs (reviewed by Wittmann, 1983) have been generally helpful in conceptualizing the spatial interactions involved in translation; however, these models are based only on a subjective synthesis from a few views of the particle and the results of immuno-electron microscopy.

Because of the large size of the ribosome, and the difficulties in obtaining well-ordered crystals of sufficient size, the progress of x-ray diffraction methods has been very slow. EM combined with techniques of image processing and three-dimensional (3D)[1] reconstruction, either applied to two-dimensional crystals (Arad et al., 1987; Yonath and Wittmann, 1989) or single particles (Radermacher et al., 1987*a*; Wagenknecht et al., 1989) has therefore been the main source of quantitative structural information.

To date, the most detailed description of 3D morphology has been obtained by application of the random-conical reconstruction technique (Radermacher et al., 1987*b*, Radermacher, 1988) to ribosomes in single particle form prepared by negative staining and air-drying. However, this preparation technique has three major limitations: (*a*) information is obtained predominantly about the surface of the particle, and little about its interior; (*b*) if uranyl salts are used, then positive staining of RNA exposed at the surface may occur, resulting in a misinterpretation of certain features; (*c*) the relatively open, highly hydrated structure evidently presented by the ribosome may collapse under the forces exerted upon it during air drying (Wagenknecht et al., 1989; Carazo et al., 1989).

By contrast, the method of cryo-electron microscopy of specimens embedded in vitreous ice (Dubochet et al., 1982) has been shown to avoid these problems, by preserving the specimen in a fully hydrated form without the help of a heavy metal contrasting agent. Interior features become visible, which can be related, in a quantitative way, to the scattering density distribution, and in turn to the electron density distribution (see Jeng et al., 1989). Given sufficient resolution, the spatial distribution of ribosomal RNA within the particle can be visualized because of the high scattering of the phosphorus atoms in the RNA backbone. To date, however, only two-dimensional crystal specimens have been imaged by using cryo-electron microscopy, and the results have been limited in resolution by crystal disorder (Arad et al., 1987; Yonath and Wittmann, 1989; for eukaryotic ribosomes, see Kuhlbrandt and Unwin, 1982; Milligan and Unwin, 1986).

We have been successful in extending the random-conical reconstruction approach to images of the *Escherichia coli* (*E. coli*) ribosome in ice. The resulting reconstruction, at 40-Å resolution, provides the most detailed quantitative description of ribosome morphology yet achieved by means of EM. The mutual arrangement of the two subunits is revealed. The intersubunit gap appears to provide ample space for the binding of the two tRNA molecules and other translational components engaged in protein synthesis. In the interiors of the two subunits, complex-shaped regions with high density stand out that are tentatively interpreted as rRNA or rRNA rich. A bridge linking the 16S and 23S rRNA components in the region of the 30S subunit "platform" is recognized.

Material and Methods

Experimental Material

E. coli MRE-600 cells (Grain Processing, Muscatine, Iowa) are ground

1. *Abbreviations used in this paper*: CTF, contrast transfer function; 3D, three-dimensional; EM, electron microscope.

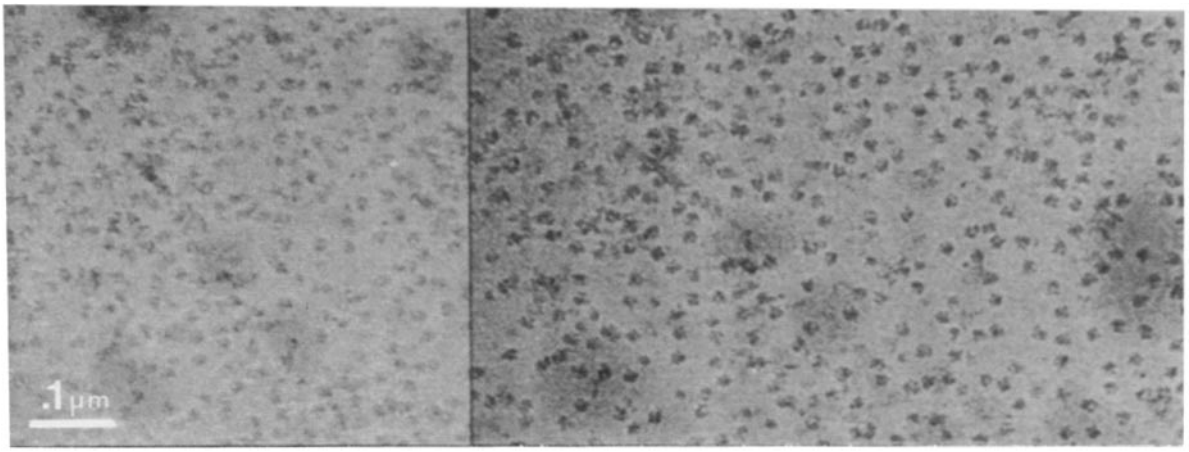

Figure 1. EM of ribosomes embedded in ice. (*Left*) Electron micrograph of specimen tilted by 50°. (*Right*) the same specimen field, untilted.

with alumina and the ribosomes are extracted into a buffer consisting of 20 mM tris-HCl (pH 7.5), 10 mM $MgCl_2$, 100 mM NH_4Cl, 0.5 mM EDTA, and 3 mM β-mercaptoethanol. Tight-couple 70S ribosomes are prepared by ultracentrifugation of alumina extract in a Ti-60 rotor at 30,000 rpm for 15 h (Robertson and Wintermeyer, 1981). The inactive ribosomes are removed from the ribosomal fraction by sucrose density gradient centrifugation (10–30% wt/vol sucrose in 20 mM Tris (pH 7.5), 5.5 mM $MgCl_2$, 100 mM NH Cl, 0.5 mM EDTA, 3 mM β-mercaptoethanol).

Before EM, ribosomes were tested for their protein synthesizing capability according to the procedure of Staehelin and Maglott (1971) and were found to be 79% active. In addition, A- and P-site tRNA binding to 70S ribosomes was tested as reported by Rheinberger et al. (1988). P-site binding to 70S was confirmed by covalent cross-linking of val-$tRNA^{val}$ in the presence of poly (U_2G) (Ofengand and Liou, 1981) as well as by puromycin reaction. The incorporation was found to be 0.6 tRNA molecule/ribosome. The A-site binding obtained under similar conditions was 0.4 tRNA molecule/ribosome.

Cryo-electron Microscopy

We closely followed the experimental procedure of Wagenknecht et al. (1988) using GATAN cryo-transfer equipment and goniometer stage (model EM420; Philips Electronic Instruments, Inc., Mahwah, NJ). Copper grids (400-mesh) are covered with a thick carbon film, containing holes, on which a thin carbon film (~100 Å) is applied. The grids are glow discharged in the presence of amylamine. The particles are then applied to the specimen grids and frozen by the blotting technique (Dubochet et al., 1982) using a liquid ethane slush as freezing medium.

In our method of data collection and reconstruction (Radermacher et al., 1987*b*; Radermacher, 1988) we make use of preferred orientations of the particles on a support film. When the specimen is tilted, the particles adhering to the grid in a preferred orientation present a conical range of projections, from which an averaged particle can be reconstructed in three dimensions. In practice, each specimen field is imaged twice, first with the specimen tilted by 50° under low-dose conditions, and then with the specimen untilted. The purpose of the second micrograph is twofold: to allow the rotation angles among the particles to be determined, and to allow classes of particles presenting identical orientations to be selected by classification techniques (see below). Thus the images are taken in pairs (0°/50°) at 2 μm defocus, 36,000× magnification, and low-dose conditions (6–8 electrons/Å). At 50°, the range of defocus across the tilted field is 1.5 to 2.5 μm.

Image Processing

For image processing, the micrographs are digitized using a flatbed microdensitometer (PDS 1010A; Perkin-Elmer Corp., Norwalk, CT) with a 20 μm square scanning aperture (corresponding to 5.6 Å on the specimen scale). Particle images are simultaneously selected from the 0-degree and 50-degree micrographs displayed side-by-side on a workstation, using an interactive particle selection program (Radermacher, 1988) that establishes the geometric relationship (in terms of rotation, translation, direction of tilt axis, and tilt angle) between the two micrographs. The 0-degree images are subjected to alignment (Frank et al., 1981), multivariate statistical analysis (Van Heel and Frank, 1981), and hierarchical ascendant classification using complete linkage (see Frank, 1990). For classes containing sufficient numbers of particles, the corresponding tilt images are used for reconstruction according to the random-conical geometry. The reconstruction uses an iterative scheme (Penczek and Frank, 1991) that is based on minimizing the functional $L = W + \lambda C$, where W, the cost criterion, is the sum of squares of the reconstructed object, C is the chi-squared discrepancy between the reprojected reconstruction and the known data, and λ is a weighting factor, chosen in such a way that the discrepancy at the minimum of L is close to its expected value.

The resulting reconstructions are low-pass filtered using a radius of 1/40 $Å^{-1}$ in accordance with a phase-residual consistency test (Frank et al., 1981). For interpreting the results we use both solid-body surface representations (Radermacher and Frank, 1984) and vector-graphical displays of 3D contours on a workstation (Silicon Graphics, Mountain View, CA) using INSIGHT (Biosym Technologies, San Diego, CA) software. Only the latter-type displays are shown in this paper.

Results

The Ribosome Reconstructed from Particles in Different Views

The micrographs (typical field, see Fig. 1) show a high

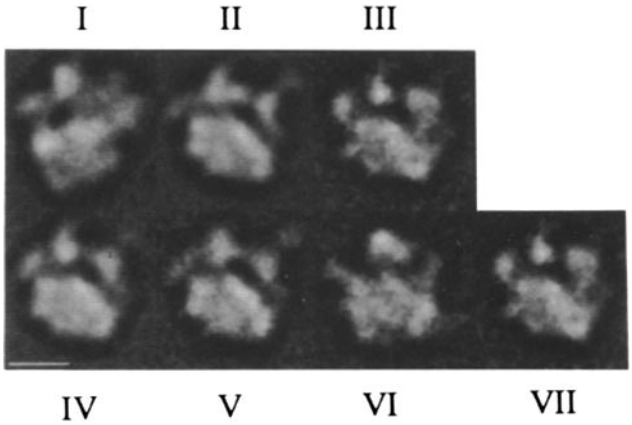

Figure 2. Averages of seven major groups (ranked by number of images) of 0°-projections showing the ribosome in three different orientations on the carbon grid. Only tilted-specimen projections belonging to groups I–III were used for separate reconstructions. Bar, 100 Å.

amount of noise, and it therefore proved difficult to use the established methods of alignment (Frank et al., 1981) without biasing the results by the choice of the alignment reference. A new reference-free algorithm was developed (Penczek and Frank, 1991) to align the set of 0°-particle images. After alignment, the images were subjected to multivariate statistical analysis and classification. Basically the images were found to fall into seven classes (Fig. 2), and we hypothesized that these classes represent different preferred orientations of the particle. Of the seven classes, the three with highest memberships (93, 144, and 66, designated I, II, and III, respectively) were chosen for separate 3D reconstructions. Two of the corresponding 0° averages (Fig. 2) resemble the views previously identified in negative stain preparations (Verschoor et al., 1986). Classes II and III clearly fall into the O-to-R range of views described in that study, whereas class I has not previously been reported.

Using a 3D search program (Penczek and Frank, 1991), we were able to find the matching orientations, in terms of Eulerian angles ψ, θ, and φ, as defined by the maximum of the cross-correlation coefficient. The "rocking" angle θ was found to be 71° between reconstructions I and II, 80° between I and III, and −10° between II and III. On the basis of a phase residual calculation, we estimated the resolution to be in the range of 40 Å. The reconstructions, brought into matching orientations with the aid of a 3D search program and low-pass filtered to 40 Å, are remarkably similar in shapes and the mutual orientations of the two easily recognizable subunits. A comparison of equivalent sections of the three reconstructions (Fig. 3, *I–III*) brings out the close correspondence of the interior density distributions. This high degree of consistency among the reconstructions, also reflected by mutual correlation coefficients close to 0.8, makes it virtually certain that the three classes of images represent a single structure lying in different orientations, and rules out the presence of significant orientation-dependent deformations. The remaining differences can be attributed to residual noise and to the different orientations of the "missing cone" relative to the particle. It is therefore justified to combine all three data sets in a merged reconstruction, by assigning appropriate Eulerian angles to the projections. Because of the large angles between the class I reconstruction and the remaining two reconstructions, the merged-data reconstruction achieves virtually complete coverage of the angular range with data, so that artifacts due to the "missing cone" are all but eliminated.

The Merged Reconstruction

A slice of the final, merged-data reconstruction (Fig. 3, *M*) shows three regions with different densities: (*a*) low density in the exterior, due to ice; (*b*) a medium-density region within the apparent particle boundaries; and (*c*) a region of high density. Because of the high amount of defocusing, some caution must be exercised in interpreting the results in terms of internal density variations within the ribosome. Observed variations could be due to the action of the contrast transfer function (CTF) for a particle whose density distribution is homogeneous, at the resolution of this study. It proved difficult to apply a CTF correction (e.g., Toyoshima and Unwin, 1988) because of a strong low-resolution peak in the power spectrum probably because of inelastic scattering, whose relative strength is related to the thickness of the ice.

Figure 3. Corresponding slices of reconstructions I–III after orientation match and of merged reconstruction (*M*). Bar, 100 Å.

A model computation showed, however, that the observed variations cannot be explained on the basis of CTF imaging of a particle with identical shape but uniform internal density. Density variations in the image showed a different pattern, and were of smaller magnitude than those reported here.

Although some distortion of the mass distribution cannot be ruled out, it seems likely that the division into medium- and high-density regions is because of the higher scattering density of ribosomal RNA (= 1.15 relative to glucose according to Kuhlbrandt and Unwin, 1982; Kuhlbrandt, 1982) as compared to the lower scattering density of protein (0.94 in the same units). (These authors found a spatial segregation of the reconstructed 80S ribosome mass at 60–70Å resolution into regions of different densities, and interpreted these results in terms of rRNA vs. ribosomal protein distribution; see Discussion.)

On the basis of this division, which will be quantified in the following, we have derived two 3D contours: one of the entire ribosome particle, and one of a putative rRNA-rich mass contained within it. Obviously, under the limitations of high-defocus bright-field imaging, which is known to cause loss of both high- and low-spatial frequency information, it is not possible to make an unambiguous determination of the density boundaries. In fact, the very concept of a density boundary and its depiction as a "hard" surface are at odds with the limited resolution. Following the practice of x-ray crystallography, we make use of a surface in the visualization of 3D density with the implicit understanding that it represents an estimated median boundary within a "shell of uncertainty," whose thickness corresponds to the resolution. Thus, any boundary specified in the following should be understood as being accompanied by margins of 20-Å thickness on either side. It is important to realize that the resolution limitation (Fourier series termination) introduces an ambiguity in the attempt to distinguish regions of an object according to scattering density: in the 3D image, any high-density feature will be encased in a layer of medium density. For instance, a particle composed of pure RNA imaged under these conditions would appear as a high-density mass surrounded by a layer ~20-Å thick of medium density "protein." While the determination of the outer particle boundary is facilitated by the contrast with ice, the placement of the inner boundary must remain tentative. Arguments for the choice of the approximate inner boundary density are put forth below (in fact, three different observations suggest the same density value). In addition, the validity of the putative rRNA distribution must also be scrutinized by comparison with the results from other experiments, as will be done later in the Discussion section.

A histogram of the reconstructed ribosome (Fig. 4) is dis-

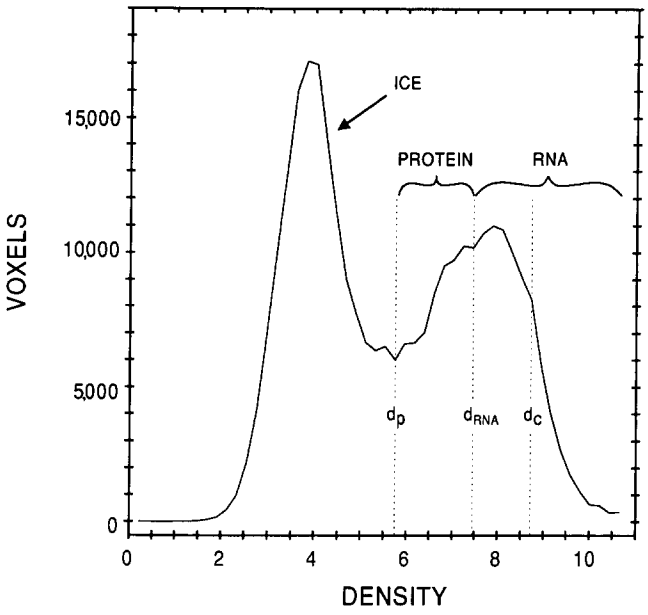

Figure 4. Histogram of 3D density distribution within the merged reconstruction. The ice peak is clearly distinguishable from the particle-related portion of the histogram by a dip (density d_p). Density d_{RNA} was considered the most likely division between protein and regions rich in ribosomal RNA. In addition, density d_c was used as threshold to visualize "core" of RNA distribution. Accordingly, the data range is divided into the three ranges designated ice, protein, and RNA.

tinctly bilobed, with a sharp narrow lobe attributed to ice and a broad lobe encompassing both the medium- and high-density regions of the particle proper. The marked dip in the curve between the two lobes (d_p in Fig. 4) may be used to define the particle boundary (see below). The broad lobe shows an indication of a division (d_{RNA}) roughly halfway within its density range. Visual inspection of a slice (Fig. 3 *d*) also places the boundary between high and medium density into the vicinity of d_{RNA}. Furthermore, the location of this density value within the particle-related portion of the histogram agrees with the volume ratio of 0.85:1 for rRNA/protein inferred from published molecular weights and mass densities of protein and rRNA (Wittmann, 1982). There is some uncertainty in this latter value because according to that study more than 10% of the measured molecular weight of the ribosome is not accounted for by the combined chemical weights of protein and RNA. This extra mass is attributed to the presence of spermidine and certain ions known to be bound to the ribosome. Other reasons for uncertainty come from the packing variations in loop, single-stranded, and double-stranded RNA, and from ribonucleoprotein comprising varying proportions of RNA and protein. However, despite this uncertainty, the agreement with the other observations makes density d_{RNA} acceptable as threshold for a representation of the rRNA-rich portion of the ribosome. In addition, we made use of a third representation, with a higher threshold d_c to find the "core" domains of rRNA.

In the representation of the particle using density d_p (outer magenta contour, Fig. 5, *a–d*), the large and the small subunits are clearly recognizable as two partially fused masses of density that enclose a sizable space which is accessible from two sides ("intersubunit gap" Fig. 5*a*). The width of this gap ranges from 50 to ~70 Å.

The 30S subunit portion, with its distinct head (*h*) region, bears similarity to some visually derived models (Lake, 1976; Wittmann, 1983). The platform (*p*), partially fused with the 50S subunit mass, becomes visible after a further rotation (Fig. 5 *c*). In this orientation, the 30S subunit outline corresponds to the view described by Lake (1976). The 50S subunit portion of the reconstruction (Fig. 5 *d*) resembles a low-resolution version (Radermacher et al., 1986) of a previous stain-derived reconstruction (Radermacher et al., 1987*a*), with all three protuberances clearly recognizable: the L1 ridge (*Ll*), central protuberance (*CP*), and stalk base (*S*). (The stalk component is rendered in truncated form, due to its mobility; we note, however, that a portion of the stalk is still visible in two individual reconstructions; not shown.) The mutual arrangement of the two subunits confirms earlier proposals based on visual interpretations of electron micrographs (Lake, 1976; Stoeffler and Stoeffler-Meilicke, 1986). If the 50S subunit is placed so that the central protuberance points upwards, as in Fig. 5, the 30S subunit lies in a diagonal position. The 30S subunit head makes contact with the 50S subunit in a position consistent with the crosslinking observed for S19 with L5 next to the peptidyl transferase center (Lambert and Traut, 1981) and with the location of S19 on the 30S subunit head (Olson et al., 1988).

Three-dimensional Distribution of Ribosomal RNA

The putative volume occupied by rRNA is visualized by applying density (d_{RNA}) defined above as a threshold to the reconstruction (cyan inner contours in Fig. 5, *a–d*). The resulting interior mass has a shape of high complexity, and allows for a considerable degree of interpenetration of RNA and protein. The 16S RNA of the small subunit (Fig. 5, *b* and *c*) appears as a hook-shaped mass that anticipates the overall shape of the subunit and forms the major portion of the platform. A domain that occupies 25% of the 16S rRNA is separated from the main mass. (The low resolution of this study would not allow a thin connecting structure such as a single RNA strand to be visualized.)

Within the large subunit (Fig. 5 *d*), we see a mass of convoluted shape, which we attribute largely to the 23S rRNA, noting that the small 5S RNA component is known to be packed into the central protuberance (Shatsky et al., 1980; Christiansen and Garrett, 1985). Several holes and crevices are visible in the 23S RNA.

When the structure is presented in an orientation such that the two subunits appear maximally separated (Fig. 5 *a*), two regions of contact or at least close proximity between the 16S and the 23S RNA mass become visible: one occurs as a strong "bridge" formed by an extension of the "platform" portion of the 16S RNA, linking it with RNA at the base of the L1 protein region of the large subunit, and one extends from the separate "head" domain of the 16S RNA to rRNA located within the central protuberance of the large subunit.

It is difficult to appreciate the shape of the RNA–RNA "bridge" domain without resorting to a representation of the ribosome from the top (Fig. 5 *e*), in which the RNA portion of the 30S subunit head is seen to face the RNA portion of the 50S subunit's central protuberance. It then becomes apparent that the "bridge" contact involves an extended portion

of RNA at the platform lip on the side of the small subunit and a long strand of RNA on the interface side of the 50S subunit. This latter strand runs from the base of protein L1 to the base of L7/L12, forming the lower rim of the interface canyon which was recognized in Radermacher and co-worker's (1987*a*) reconstruction of the 50S subunit. It is important to note that the "bridge" prevails even at the higher density threshold d_c. We also note that a substantial portion of RNA in the interface region is encased in a medium-density layer whose thickness is <20 Å and thus could represent the effect of low-resolution series termination in the image of RNA directly exposed to solvent/ice.

Discussion

The Shape of the Ribosome: Comparison with Other Structural Studies

Before discussing the putative RNA distribution and the location of RNA–RNA contacts, the external shape of the 70S ribosome will be briefly compared with results from other structural studies. Arad et al. (1987) obtained a reconstruction from ordered arrays of *Bacillus stearothermophilus* in aurothioglucose. We note an overall agreement with our results in the general outline of the 70S particle and in the appearance of a sizable intersubunit gap. However, Arad and co-worker's model appears to be represented at a density threshold substantially higher than the histogram-derived threshold used in our model, and lacks some of the higher-resolution features that would allow a more detailed comparison.

The only reconstructions of the *E. coli* ribosome from negatively stained single particles sandwiched between carbon films (Wagenknecht et al., 1989; Carazo et al., 1989) show the ribosome partially collapsed: the intersubunit gap is closed, and the 30S subunit is strongly flattened, while the 50S subunit apparently retains its shape as judged by comparison with the reconstruction of the 50S subunit alone. As discussed in those papers, the collapse is likely a result of forces acting upon the ribosome in the particular range of orientations which the particle assumes in the sandwich preparation. This interpretation is supported by Verschoor and Frank's (1990) recent single-particle reconstruction of the negatively stained 80S ribosome from reticulocyte, which is oriented in such a way that collapse-inducing forces are minimized. This latter reconstruction indeed bears a striking resemblance to our present results in terms of the mutual arrangement of small and large subunit and the topology of the intersubunit space. (The fact that this space is somewhat more open in the 80S ribosome than in the 70S ribosome may be a result of interkingdom variation and artifacts of negative staining.)

The comparison between the current results and those obtained with negative staining clearly indicates that the technique of frozen-hydrated EM of the unstained sample produces a better preserved 3D structure of the ribosome. However, the most important improvement is that in the unstained specimen, the discrimination between regions of the object with high and low scattering density is possible.

Spatial Distribution of rRNA

Despite the ambiguities due to limited resolution and CTF effects, the model we present is more specific than previous studies in pinning down the spatial distribution of ribosomal RNA. Is this distribution consistent with what is known from other studies? There are four types of data with which we can compare our results: (*a*) those obtained by directly imaging rRNA components of the *E. coli* ribosome; (*b*) those obtained by imaging the phosphorus characteristic for the RNA backbone; (*c*) results obtained by contrast matching; and (*d*) models obtained on the basis of inferred RNA secondary structure and cross-linking information. In addition, some constraints are set by the radii of gyration found by low-angle scattering studies and the protein locations known from neutron scattering.

Direct Imaging. The first type of experimental results, notably those obtained by Vasiliev's group (1986), was obtained by EM of 16S and 23S rRNA particles that were freeze dried and shadowed. Comparison of these unaveraged images with our results is difficult because of a great degree of variation, and because the precise viewing angle is not known. Nevertheless, there is a similarity in the basic shapes of both the 16S and 23S rRNA particles in published micrographs (Vasiliev et al., 1986) and certain projections of the corresponding masses distinguished in the present reconstruction: the 16S particle has an asymmetric Y-shape, and the 23S particle has the characteristic shield shape, apparently the precursor of the crown view of the large subunit. On the other hand, the value of these results in the present comparison is somewhat weakened by indications of large conformational variations and compaction of rRNA upon association with ribosomal proteins (Mandiyan et al., 1989).

Phosphorus Imaging. An image of the 16S RNA component of the 30S subunit was recently obtained by Boublik et al. (1990) by using the scanning transmission electron microscope in a mode sensitive to atomic number. This image closely resembles a projection of our putative 16S RNA distribution when presented with a viewing angle between those used in Figs. 5 *a* and *b* (data not shown). Both 16S and 23S RNA components were earlier studied by Korn et al. (1983) by spectroscopic imaging in the transmission electron microscope equipped with an energy filter. In their images, the outer shapes of the subunits are not well defined, and the 16S RNA component appears in a variety of shapes. However, the image of the 23S component obtained by these authors is reminiscent of the corresponding mass in our reconstruction when the latter is presented at the high (d_c) density level, showing a complex shape with distinct strands and holes. Apart from providing confirmation for the overall shapes of the putative 16S and 23S masses in our study, these findings indicate, in support of our results, that RNA-rich mass is concentrated over regions large enough to be observed by EM.

Imaging by Contrast Matching. A visualization of rRNA within the eukaryotic ribosome was accomplished by Kuhlbrandt and Unwin (1982) by a contrast-matching technique (Kuhlbrandt, 1982). Although limited in resolution to 60 to 70 Å, the results of this study clearly show evidence of a concentration of a mass with higher scattering density, as expected for RNA, towards the center of the particle. This finding agrees with the more compact distribution of our putative RNA masses within each subunit, and their asymmetric positions which place them closer to the interface than to the solvent sides (see Fig. 5 *a*).

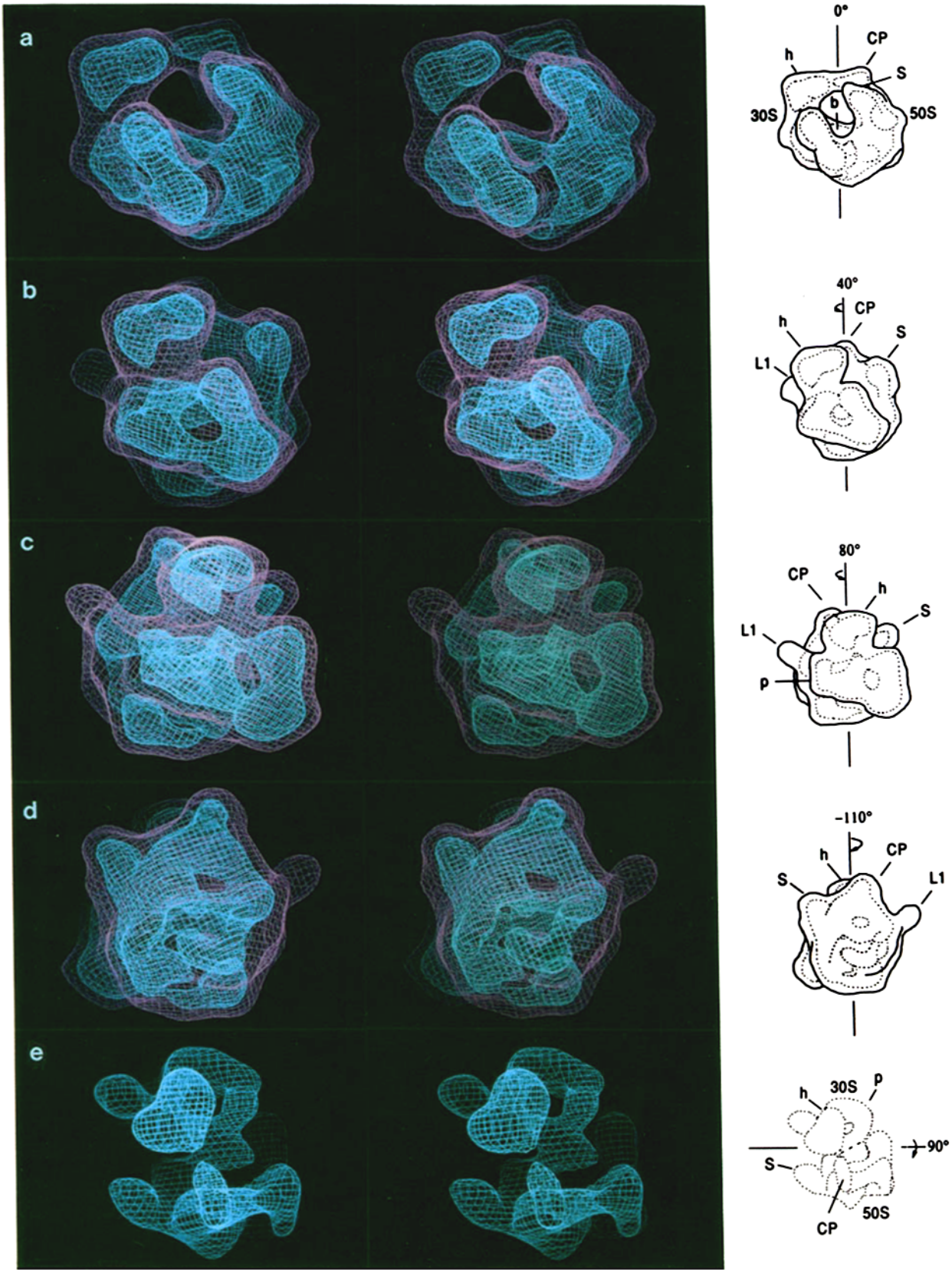

Figure 5. Computer-graphical representation of merged reconstruction in stereo view. Magenta: surface d = d_p, representing the outer envelope of the particle (interface ice/protein); cyan: surface d = d_{RNA}, representing the envelope of ribosomal RNA (approximate interface protein/RNA). The views (*b–d*) were produced by rotating the ribosome around the vertical axis by the angles ϕ indicated. Meaning of symbols in 30S subunit: *h* = head, *p* = platform; 50S subunit: *Ll* = L1 arm, *S* = stalk base, *CP* = central protuberance; *b* = "bridge" region where 16S RNA and 23S RNA are in close contact. (*a*) Side view, showing 30S and 50S subunits partially separated by a gap

RNA Folding Models. This type of data is obtained from attempts to integrate secondary structure information, intra-RNA cross-linking information, and RNA-protein cross-linking, considering the protein locations inferred by neutron scattering and immuno-electron microscopy. The resulting models are currently rather speculative, which can be seen from the conflicting results obtained by different groups (Expert-Bezancon and Wollenzien, 1985; Brimacombe et al., 1988; Stern et al., 1988; Malhotra et al., 1990). Platform, body, and head domains can always be distinguished, but this agreement can be attributed to the use of similar subunit models derived from EM data. Interestingly, Stern and co-worker's (1988) model shows a distinct head domain well separated from the other domains, a feature not shared by the models of the other groups, but in agreement with the mass distribution found in our study. Based on the number of residues in Stern and co-workers' (1988) 30S head domain, it should occupy roughly 1/3 of the total 16S RNA volume. By comparison, we found the head domain in our reconstruction to occupy 1/4 of the total 16S RNA mass at threshold level d_{RNA}.

Furthermore, on the basis of cross-linking studies and what is known about the 30S subunit morphology, Oakes et al. (1990) arrived at the conclusion that the platform is formed by a ring of RNA. In fact, the RNA-rich mass we have found forms a ring and thereby defines the platform. In Fig. 5 *c*, this ring is seen in a horizontal position, slightly from above. In Fig. 5 *e*, the ring appears as the most striking feature of the high-density mass within the 30S subunit.

Low-angle Scattering Studies. Some information on the relative spatial distribution of protein and RNA is available from low-angle scattering. A recent study of the 30S subunit (Ramakrishnan, 1986) shows that the radii of gyration of protein and 16S RNA are closely matched (70 and 68 Å, respectively) when nonribosomal proteins and excess protein S1 are removed by salt washing. This indicates that the subunit definitely cannot be modeled as a core of RNA to which protein is peripherally attached. However, this finding still permits many configurations in which RNA is highly localized, forming sizable regions between which protein is situated. Specifically, it is not inconsistent with our interpretation, as a direct radius of gyration computation shows, applied to a volume in which the small subunit was isolated by using a cutting plane: for the putative distributions of 16S RNA and 30S protein, the radii of gyration were indeed found to be matched within 2%, at an average value of 63Å. In other words, while low-angle scattering indicates that the proteins and RNA are intermingled in the 30S subunit (as stated by Ramakrishnan, 1986), the "coarseness" with which homogeneous regions of the two components appear in this mixture cannot be derived from such measurements. The particular mixture we have found is one of the many consistent with a finding of matching radii of gyration.

For the 50S subunit, the radius of gyration was always found to be substantially larger for protein than for RNA (e.g., Crichton et al., 1977; Serdyk and Grenader, 1975). This is consistent with the appearance of RNA within the large-subunit portion of our reconstruction as a relatively compact mass.

Protein Locations from Neutron Scattering. The most detailed picture of ribosomal protein locations within the small subunit has been obtained by neutron scattering (Moore et al., 1985; Capel et al., 1988). These studies are able to pinpoint the centers of gravity of proteins, and thereby produce constraints for the locations of known protein–RNA crosslinking sites. However, they do not allow specific low-resolution models of RNA distribution to be excluded, other than those which, unlike ours, present the RNA component concentrated in a compact core.

23S RNA: Relationship to Other Imaging Studies. The complex shape of the putative rRNA mass within the 50S subunit requires a detailed interpretation, but currently very little is known about the secondary and tertiary structure of the 23S RNA. It is tempting to identify the three pronounced holes seen in this mass with some features recognized in previous electron microscopic studies. The "tunnel" reported by Yonath and Wittmann (1987) in the large ribosomal subunit of *B. stearothermophilus* could in fact be a low-resolution version of the most pronounced hole, represented with a high threshold that essentially excludes the ribosomal protein. Two of these holes occur at positions that closely match the holes visible in Radermacher et al. (1987*a*) 50S subunit reconstruction from negatively stained specimens when visualized at elevated density thresholds (Frank et al., 1990).

RNA–RNA Interaction

The most interesting specific feature of our reconstruction is the appearance of two evident points of RNA–RNA contact or close proximity: the "bridge" linking RNA within the 30S platform with RNA close to the base of L1, and the close proximity of the RNA domain in the 30S head domain to RNA in the central protuberance. The resolution of this study makes it difficult to ascertain whether or not actual contact occurs at either point; however, the fact that the "bridge" remains intact at the higher density threshold makes it very likely that it represents a region where close interaction between the two rRNA components takes place, and that it has an important function in the subunit association. In fact, 16S and 23S RNA associate in the absence of protein to form a complex under conditions that are known to induce assembly of ribosomes (Burma et al., 1983). This assembly is functional to a significant extent in several steps of protein synthesis (Burma et al., 1985).

According to Herr et al. (1979) and Vassilenko et al. (1981), the residues that are found at position 337, the 790 loop region and the region 1389-1390 of 16S RNA contain sites that make contact with the 50S subunit and are essential for subunit association. Residue sequences that fall in these regions have recently been mapped by Oakes and Lake

("interface gap") and the location of a bridge b connecting 16S and 23S RNA masses; (*b* and *c*) cytoplasmic views (i.e., from the solvent-accessible side) of 30S subunit from two different directions (ϕ = 40° and 80°, respectively); (*d*) cytoplasmic view of 50S subunit (ϕ = −110°); (*e*) top view down the long axis of 30S subunit, showing only RNA contour and revealing connecting "bridge." This view was generated by rotating the ribosome from position (*d*) by 90° around the horizontal axis. *Dashed line*, demarcation of boundary between the two subunits.

(1990) to the platform region of the small subunit. These results agree with the location of the RNA-RNA "bridge" as an extension of the platform. Residues 1492 to 1505, which fall into the cleft of the small subunit, in close vicinity to the platform region (Oakes and Lake, 1990), have also been implicated in the association of the subunits. Other chemical modification experiments that have a bearing on subunit association have been reviewed by Raue et al. (1990). In this context it is interesting to note that the folding model by Stern et al. (1988) predicts that 16S sites presumed to interact with the 50S subunit are highly localized in the platform region, on the side where the connecting "bridge" of our reconstruction is seen.

Our results have many implications as to the location of functional sites involved in t-RNA binding and translocation, since it provides new spatial constraints for these mechanisms. Numerous studies have pointed to the important function of both 16S and 23S RNA in all steps of protein synthesis. The specific RNA sequence domains that constitute the subunit interface have for instance been mapped by Meier and Wagner (1985). It is therefore tempting to proceed to construct a specific model of the entire translation mechanism (cf. Noller et al., 1990) incorporating the new information. However, such conclusions could only be tentative as long as they are not accompanied by 3D mapping using the same method with which this study was undertaken. Currently we are exploring the feasibility of extending this study to a complete translational system in which the ribosome is in defined states of processing.

In conclusion, the reconstruction of the ribosome in ice has revealed a surprising amount of information especially on the internal distribution and contact points of ribosomal RNA despite the limited spatial resolution. Even though the interpretation of the internal high-density mass as RNA or RNA rich does not rest on a positive identification of RNA by imaging—which would require either spectroscopic imaging or the use of chemical labels—the distribution found by application of a threshold is both plausible and consistent with the results of numerous studies.

We expect to be able to overcome the present resolution limitation by combining data from differently defocused micrographs, a technique already successfully used for crystals (Toyoshima and Unwin, 1988). At the same time, a correction of the CTF will enable us to delineate the boundary of rRNA in both subunits with higher fidelity. 3D visualization of ligand binding in functional studies of the fully hydrated ribosome now appears feasible.

We thank Michael Radermacher, Terence Wagenknecht, and Adriana Verschoor for many valuable suggestions and extensive discussions. We are grateful to Witold Grochulski (Purdue University, Lafayette, IN) for a discussion of the 3D reconstruction technique. We received technical assistance from Michael Marko and Ardean Leith. Finally we thank Stephen Bryant for the use of his Silicon Graphics workstation, for his help with the display of the model, and a critical reading of the manuscript.

This work was supported by grants National Institutes of Health 1R01 GM29169 and NSF National Science Foundation PCM-8313045.

References

Arad, T., J. Piefke, S. Weinstein, H.-S. Gewitz, A. Yonath, and H. G. Wittmann. 1987. Three-dimensional image reconstruction from ordered arrays of 70S ribosomes. *Biochimie (Paris).* 69:1001–1006.

Boublik, M., V. Mandiyan, S. Tumminia, J. F. Hainfeld, L. D. Peachey, and J. S. Wall. 1990. Structural analysis of ribosomal particles from Escherichia coli by scanning transmission electron microscopy. *In* Proc. XII Int. Congr. Electron Microscopy, L. D. Peachey, and D. B. Williams, editors. San Francisco Press, Vol. III, 134–135.

Burma, D. P., B. Nag, and D. S. Tewari. 1983. Association of 16S and 23S ribosomal RNAs to form a biomolecular complex. *Proc. Natl. Acad. Sci. USA.* 80:4875–4878.

Burma, D. P., D. S. Tewari, and A. K. Srivastava. 1985. Ribosomal activity of the 16S-23S RNA complex. *Arch. Biochem. Biophys.* 239:427–435.

Capel, M. S., M. Kjeldgaard, D. M. Engelman, and P. B. Moore. 1988. Positions of S2, S13, S16, S19, and S21 in the 30S ribosomal subunit of *Escherichia coli. J. Mol. Biol.* 200:65–87.

Carazo, J. M., T. Wagenknecht, and J. Frank. 1989. Variations of the three-dimensional structure of the *Escherichia coli* ribosome in the range of overlap views. *Biophys. J.* 55:465–477.

Christiansen, J., and R. A. Garrett. 1986. How do protein L18 and 5S RNA interact? *In* Structure, Function and Genetics of Ribosomes. B. Hardesty, and G. Kramer, editors. Springer-Verlag Inc., New York, New York. 253–269.

Crichton, R. R., D. M. Engelman, J. Haas, M. H. J. Koch, P. B. Moore, R. Parfait, and H. B. Sturmann. 1977. *Proc. Natl. Acad. Sci. USA.* 74:5547–5550.

Dubochet, J., J. Lepault, R. Freeman, J. A. Berriman, and J. C. Homo. 1982. Electron microscopy of frozen water and aqueous solutions. *J. Microscopy.* 128:219–237.

Durani, T. S., and C. E. Goutis. 1980. Optimization techniques for digital image reconstruction from their projections. *Institution of Electrical Engineers (Lond.) Proc.* 127E:161–169.

Frank, J. 1990. Classification of macromolecular assemblies studied as "single particles." *Quart. Rev. Biophys.* 23:281–329.

Frank, J., A. Verschoor, and M. Boublik. 1981. Computer averaging of electron micrographs of 40S ribosomal subunits. *Science (Wash. DC).* 214:1353–1355.

Frank, J., A. Verschoor, M. Radermacher, and T. Wagenknecht. 1990. Morphologies of eubacterial and eucaryotic ribosomes as determined by three-dimensional electron microscopy. *In* Ribosome—Structure, Function, & Evolution. E. Hill, A. Dahlberg, R. A. Garrett, P. B. Moore, D. Schlesinger, and J. R. Warner, editors. American Society of Microbiology. Washington, D.C. 107–113.

Herr, W., N. M. Chapman, and H. F. Noller. 1979. Mechanism of ribosomal subunit association: discrimination of specific sites in 16S RNA essential for association activity. *J. Mol. Biol.* 130:433–449.

Jeng, T.-W., R. A. Crowther, G. Stubbs, and W. Chiu. 1989. Visualization of alpha helices in TMV by cryo-electron microscopy. *J. Mol. Biol.* 205:251–257.

Korn, A. P., P. Spitnik-Elson, D. Elson, and F. P. Ottensmeyer. 1983. Specific visualization of ribosomal RNA in the intact ribosome by electron spectroscopic imaging. *Eur. J. Cell Biology.* 31:334–340.

Kuhlbrandt, W. 1982. Discrimination of protein and nucleic acids by electron microscopy using contrast variation. *Ultramicroscopy.* 7:221–232.

Kuhlbrandt, W., and P. N. T. Unwin. 1982. Distribution of RNA and Protein in crystalline eukaryotic ribosomes. *J. Mol. Biol.* 156:431–448.

Lake, J. A. 1976. Ribosome structure determined by electron microscopy of *Escherichia coli* small subunits and monomeric ribosomes. *J. Mol. Biol.* 105:131–159.

Lambert, M. J., and R. R. Traut. 1981. The subunit interface of the *Escherichia coli* ribosome: identification of proteins at interface between the 30S and 50S subunit by crosslinking with 2-iminothiolane. *J. Mol. Biol.* 149:451–479.

Malhotra, A., R. K.-Z. Tan, and S. C. Harvey. 1990. Prediction of the three-dimensional structure of *Escherichia coli* 30S ribosomal subunit: a molecular mechanics approach. *Proc. Natl. Acad. Sci. USA.* 87:1950–1954.

Mandiyan, V., S. Tumminia, J. S. Wall, J. F. Hainfeld, and M. Boublik. 1989. Protein-induced conformational changes in 16S ribosomal RNA during the initial assembly steps of the *Escherichia coli* 30S ribosomal subunit. *J. Mol. Biol.* 210:323–336.

Milligan, R. A., and P. N. T. Unwin. 1986. Location of exit channel for nascent protein in 80S ribosome. *Nature (Lond.).* 319:693–695.

Moore, P. B., M. Capel, M. Kjeldgaard, and D. M. Engelman. 1985. A 19 protein map of the 30S ribosomal subunit of *Escherichia coli.* In Structure, Function, and Genetics of Ribosomes. B. Hardesty, and G. Kramer, editors. Springer-Verlag New York Inc., New York. 87–100.

Noller, H. F., D. Moazed, S. Stern, T. Powers, P. N. Allen, J. M. Robertson, B. Weiser, and K. Triman. 1990. Structure of rRNA and its functional interactions in translation. *In* The Ribosome. Structure, Function, and Evolution. W. E. Hill, A. Dahlberg, R. A. Garrett, P. B. Moore, D. Schlesinger, and J. R. Warner, editors. American Society for Microbiology. Washington, D.C., 73–92.

Oakes, M. I., and J. A. Lake. 1990. DNA-hybridization electron microscopy. Localization of five regions of 16S rRNA on the surface of the 30S ribosomal subunits. *J. Mol. Biol.* 211:897–906.

Ofengand, J., and R. Liou. 1981. Correct codon-anticodon base paring at 5'-anticodon position blocks covalent cross-linking between transfer ribonucleic acid and 16S RNA at ribosomal P site. *Biochemistry.* 20:552–559.

Olson, H. M., T. V. Olah, B. S. Cooperman, and D. G. Glitz. 1988. Immune electron microscopy localization of dinitrophenyl-modified ribosomal pro-

tein S19 in reconstituted *Escherichia coli* 30S subunit using antibodies to dinitrophenol. *J. Biol. Chem.* 263:4801–4806.
Penczek, P., and J. Frank. 1991. Three-dimensional reconstruction of single particles embedded in ice. *Ultramicroscopy*. In press.
Radermacher, M. 1988. Three-dimensional reconstruction of single particles from random and non-random tilt series. *J. Electron Microsc.* 9:359–394.
Radermacher, M., and J. Frank. 1984. Representation of three-dimensional reconstructed objects in electron microscopy by surfaces of equal density. *J. Microsc.* 136:77–85.
Radermacher, M., T. Wagenknecht, A. Verschoor, and J. Frank. 1986. A new reconstruction scheme applied to 50S ribosomal subunit of *E. coli*. *J. Microscopy.* 141:RP1–RP2.
Radermacher, M., T. Wagenknecht, A. Verschoor, and J. Frank. 1987*a*. Three-dimensional structure of the large ribosomal subunit from *Escherichia coli*. *EMBO (Eur. Mol. Biol. Organ.) J.* 6:1107–1114.
Radermacher, M., T. Wagenknecht, A. Verschoor, and J. Frank. 1987*b*. Three-dimensional reconstruction from a single-exposure random conical tilt series applied to the 50S ribosomal subunit of *Escherichia coli*. *J. Microscopy.* 146:113–136.
Raue, H. A., W. Musters, C. A. Rutgers, J. Van 'TRiet, and R. J. Planta. 1990. rRNA: from structure to function. *In* The Ribosome – Structure, Function, and Evolution. W. E. Hill, A. Dahlberg, R. A. Garrett, P. B. Moore, D. Schlesinger, and J. R. Warner, editors. American Society for Microbiology, Washington, D.C. 217–235.
Reinberger, H. J., U. Geigenmullar, M. Wedde, and K. H. Nierhaus. 1988. Ribosomal elongation cycle: tRNA binding, translocation and tRNA release. *Methods Enzymol.* 164:658–670.
Robertson, M. J., and W. Wintermeyer. 1981. Effect of translocation on topology and conformation of anticodon and D loops of $tRNA^{phe}$. *J. Mol. Biol.* 151:57–79.
Serdyuk, I. N., and A. K. Grenader. 1975. Joint use of light, x-ray and neutron scattering for investigation of RNA and protein mutual distribution within the 50S subparticle of *E. coli* ribosomes. *FEBS (Fed. Eur. Biochem. Soc.) Lett.* 59:133–136.
Shatsky, I. N., A. G. Evstafieva, T. F. Bystrova, A. A. Bogdanov, and V. D. Vasiliev. 1980. Topography of RNA in the ribosome: location of the 3′ end of 5S RNA on the central protuberance of the 50S subunit. *FEBS (Fed. Eur. Biochem. Soc.) Lett.* 121:97–100.
Staehelin, T., and D. R. Maglott. 1971. Preparation of *E. coli* ribosomal subunit active in polypeptide synthesis. *Methods Enzymol.* 22:449–456.
Stern, S., B. Weiser, and H. F. Noller. 1988. Model for the three-dimensional folding of 16S ribosomal RNA. *J. Mol. Biol.* 204:447–481.
Stoeffler, G., and M. Stoeffler-Meilicke. 1980. Immuno electron microscopy on *Escherichia coli* ribosomes. *In* Structure, Function, and Genetics of Ribosomes. B. Hardesty, and G. Kramer, editors. Springer-Verlag New York Inc., New York. 28–46.
Toyoshima, C., and N. Unwin. 1988. Ion channel of acetylcholine receptor reconstructed from images of postsynaptic membranes. *Nature (Lond.)* 336:247–250.
Van Heel, M., and J. Frank. 1981. Use of multivariate statistics in analyzing images of biological macromolecules. *Ultramicroscopy.* 6:187–194.
Vassilenko, S. K., P. Carbon, J. P. Ebel, and C. Ehresmann. 1981. Topography of 16S RNA in 30S subunits and 70S ribosomes; accessibility to cobra venom nuclease. *J. Mol. Biol.* 152:699–721.
Vasiliev, V. D., I. N. Serdyuk, A. T. Gudkov, and A. S. Spirin. 1986. Self-organization of ribosomal RNA. *In* Structure, Function, and Genetics of Ribosomes. B. Hardesty, and G. Kramer, editors. Springer-Verlag New York Inc., New York. 128–142.
Verschoor, A., and J. Frank. 1990. Three-dimensional structure of the mammalian cytoplasmic ribosome. *J. Mol. Biol.* 214:737–749.
Verschoor, A., J. Frank, M. Radermacher, T. Wagenknecht, and M. Boublik. 1984. Three-dimensional reconstruction of the 30S ribosomal subunit from randomly oriented particles. *J. Mol. Biol.* 178:677–698.
Verschoor, A., J. Frank, T. Wagenknecht, and M. Boublik. 1986. Computer-averaged views of the 70S monosome from *Escherichia coli*. *J. Mol. Biol.* 187:581–590.
Wagenknecht, T., R. Grassucci, and J. Frank. 1988. Electron microscopy and computer image averaging of ice-embedded large ribosomal subunits from *Escherichia coli*. *J. Mol. Biol.* 199:137–147.
Wagenknecht, T., J. M. Carazo, M. Radermacher, and J. Frank. 1989. Three-dimensional reconstruction of the ribosome from *Escherichia coli*. *Biophys. J.* 55:455–464.
Wittmann, H. G. 1982. Components of bacterial ribosomes. *Annu. Rev. Biochem.* 51:155–183.
Wittmann, H. G. 1983. Architecture of prokaryotic ribosomes. *Annu. Rev. Biochem.* 52:35–65.
Yonath, A., and H. G. Wittmann. 1989. Challenging the three-dimensional structure of ribosomes. *Trends Biochem.* 14:329–335.
Yonath, A., K. R. Leonard, and H. G. Wittmann. 1987. A tunnel in the large ribosomal subunit revealed by three-dimensional image reconstruction. *Science (Wash. DC).* 236:813–816.